Faraday Discussions

Cite this: *Faraday Discuss.*, 2025, **259**, 282

ROYAL SOCIETY OF CHEMISTRY

PAPER

View Article Online
View Journal | View Issue

Characterization of lipid chain order and dynamics in asymmetric membranes by solid-state NMR spectroscopy†

Oskar Engberg, Viola Döbel, Kathrin M. Engel and Daniel Huster *

Received 9th December 2024, Accepted 16th January 2025
DOI: 10.1039/d4fd00192c

We studied the structure and dynamics of asymmetric POPC^{out}/(POPE/POPG)^{in} and POPS^{out}/(POPE/POPG)^{in} lipid membranes. To this end, the outer layer of multilamellar POPE/POPG (molar ratio 9 : 1) vesicles was exchanged (using methyl-β-cyclodextrin) by either chain deuterated POPC-d_{31} or POPS-d_{31}, for which ^{2}H NMR order parameters were measured. As controls, we prepared symmetric POPC-d_{31}/POPE/POPG and POPS-d_{31}/POPE/POPG membranes of the composition of just the outer membrane of the asymmetric multilamellar vesicles and pure POPC-d_{31} or POPS-d_{31} multilamellar vesicles. Compared to symmetric membranes of the same lipid composition, chain order parameters (S) of the asymmetric preparations were higher in the upper half of the chain and lower in the lower half. This reshuffling of acyl chain order is also expressed in higher ^{2}H NMR Zeeman order relaxation rates (R_{1Z}) of the chain segments in asymmetric membranes indicating alterations in the elastic properties of asymmetric bilayers as inferred from plots of R_{1Z} *vs.* S^2. Asymmetric membranes showed increased stiffness and rigidity although the lipid acyl chain composition between the inner and outer leaflets were identical. There were no indications for chain interdigitation between the two leaflets in the NMR spectra, which led us to speculate that the interleaflet coupling could be accomplished by sensing the differences in lipid packing densities between the two leaflets. These alterations in leaflet properties should have consequences for lipid protein interaction and ultimately protein function.

1 Introduction

The overwhelming lipid variety and asymmetry of the plasma membrane remains one of the most enigmatic characteristics of biological cells.[1,2] The energetic cost of synthesizing hundreds of different lipid species and maintaining an entropically unfavorable leaflet asymmetry of the plasma membrane is enormous and

Institute of Medical Physics and Biophysics, University of Leipzig, Härtelstr. 16/18, D-4107 Leipzig, Germany. E-mail: daniel.huster@medizin.uni-leipzig.de

† Electronic supplementary information (ESI) available. See DOI: https://doi.org/10.1039/d4fd00192c

consumes significant resources of the cell. One would expect evolution to have optimized (*i.e.* reduced) the lipid variety, composition and structure of the most important barrier for the cell unless there are important reasons to maintain this diversity. Till this day, our understanding of how specific lipids control biological function is limited to very few species such as cholesterol, phosphatidylinositolbisphosphate (PIP_2), diacylglycerol (DAG), docosahexaenoic acid (DHA), and phosphatidylserine (PS).[3–6] For the majority of lipids, however, the biological reason for the tremendous lipid variety is still unknown. Various examples of lipid function as second messengers, "force from lipid", or specific lipid–protein interactions are known,[3–6] however, most of our knowledge has been achieved from membrane models with symmetric lipid distribution,[6–8] ignoring the most prevailing feature of all plasma membranes. But an increasing body of studies suggests that numerous core functions of the plasma membrane are related to membrane leaflet asymmetry.[9]

Recent work has demonstrated that (i) preparation of asymmetric membrane models is possible with a reasonable effort,[10] and (ii) both membrane and protein properties are sensitive to lipid asymmetry,[11–13] which provides an imperative to represent this important aspect in our membrane models for biophysical studies. The limited amount of data that is available for asymmetric membrane preparations describes numerous unique findings.[9] One such aspect is intraleaflet coupling. Differential scanning calorimetry work has revealed that asymmetric $POPC^{out}/POPE^{in}$ and $POPE^{out}/POPC^{in}$ membranes have different melting characteristics.[11] A coupled phase transition was only observed for the $POPC^{out}/POPE^{in}$ vesicles, while the $POPE^{out}/POPC^{in}$ vesicles showed the individual melting temperatures of each lipid species. Another study of symmetric and asymmetric DPPC/DPPS vesicles also showed quite different DSC thermograms.[14] Intraleaflet coupling is thought to be related to interdigitation of the lipid chains.[15] Cholesterol, although it is known for its very fast flip flop between the two membrane leaflets, has also been found to be highly asymmetrically distributed between the leaflets, where the exoplasmic leaflet contains significantly more cholesterol.[16,17] Accordingly, lipid leaflet asymmetry also influences lateral domain formation.[18] Most importantly, first studies demonstrate that membrane asymmetry influences membrane protein function.[13,19]

NMR methods along with X-ray and neutron scattering as well as FTIR spectroscopy have shaped our understanding of lipid membranes as highly dynamic entities that show a transient lateral heterogeneity.[20–24] Lipid molecules undergo multiple different motions with varying amplitudes involving timescales from ps to ms.[24] This leads to a high degree of disorder and membrane elastic properties that are designed to optimize protein function,[25–28] but also other functions like permeability, fusion, small molecule binding *etc.* As the plasma membrane is enriched in saturated lipids and cholesterol in the outer and unsaturated lipids in the inner leaflet, it has been suggested that the two leaflets have different mechanical properties.[2] Indeed, higher bending moduli were measured in asymmetric egg $sphingomyelin^{out}/POPE^{in}$ vesicles.[29] The high lipid dynamics is also very well represented in modern all atom molecular dynamics (MD) simulations, which can also be done for asymmetric systems and easily span trajectories of tens of microseconds.[30] Nevertheless, similar to the situation in experimental work, there are much fewer MD simulations on asymmetric

membranes in comparison to the huge amount of MD data on symmetric membranes.[31–33]

While the dynamic nature of lipid-induced effects on protein function has long been a matter of discussion,[25–28,34] considering the aspect of membrane asymmetry has to be taken into account in the next step. While especially scattering and some FTIR data is available for asymmetric membranes,[12,14,29,35] the powerful arsenal of NMR methods to characterize membrane properties has so far only rarely been utilized, essentially only to characterize the degree of asymmetry.[36,37] In this discussion, we present ^{2}H NMR spectroscopy data on two asymmetric membrane preparations that compare (i) acyl chain order parameters, (ii) lipid packing properties, and (iii) dynamic/elastic properties of the two leaflets of asymmetric membranes composed of monounsaturated POPE/POPG (9 : 1) in the inner leaflet and either POPC or POPS in the outer. For the asymmetric preparations, we used multilamellar vesicles (MLVs) whose outer shell is exchanged with either POPC or POPS. This allows for studying membrane properties of the outer leaflet only as all inner membranes of the MLVs are symmetric. However, using acyl chain perdeuterated lipids for the exchange, the isotopic enrichment of the outer leaflet is sufficient to study the structure and dynamics of this lipid leaflet with atomic resolution.

2 Materials and methods

1-Palmitoyl-2-oleoyl-*sn*-glycero-3-phosphocholine (POPC), 1-palmitoyl-2-oleoyl-*sn*-glycero-3-phosphoethanolamine (POPE), 1-palmitoyl-2-oleoyl-*sn*-glycero-3-phospho-(1′-*rac*-glycerol) (POPG), and 1-palmitoyl-2-oleoyl-*sn*-glycero-3-phospho-L-serine (POPS) were purchased from Avanti Polar Lipids (Alabaster, AL, USA). POPC-d_{31}, and POPS-d_{31} were perdeuterated in the palmitoyl *sn*-1 chain and also purchased from Avanti. All other chemicals purchased were of the highest purity if not stated otherwise. Solvents were obtained in the highest commercially available purity from Biosolve BV (Valkenswaard, Netherlands). The chemicals 2,5-dihydroxybenzoic acid (DHB) and 9-aminoacridine (9-AA) were purchased from Sigma Aldrich (Taufkirchen, Germany) and Acros Organics (Geel, Belgium), respectively.

2.1 Asymmetric MLV sample preparation

For preparation of asymmetric membranes, we by and large followed the protocol of Doktorova *et al.*[10] with some essential modifications. Most importantly, there was no need to use sucrose as the acceptor lipid structures were MLVs, and SUVs as donor vesicles. For separation of donor and acceptor vesicles, simple centrifugation worked well. Therefore, there was no worry that sucrose could interfere with lipid structure and dynamics. An extra centrifugation step was added for easier handling of the final pellet to be transferred into an NMR rotor.

Lipids were dissolved in $CHCl_3$/MeOH (1 : 1 v/v) and evaporated at 40 °C using a rotary evaporator. The donor vesicles (composed of either POPC-d_{31} or POPS-d_{31}) were prepared at a concentration of 10 mg ml^{-1} in mqH_2O containing 35 mM NaCl and probe sonicated on ice (duty cycle 50%) until transparent (~30 min) to form small unilamellar vesicles (SUV). The acceptor vesicles were prepared from POPE/POPG (9 : 1 molar ratio) lipid mixtures suspended at a concentration of

10 mg ml^{-1} in mqH_2O containing 35 mM NaCl and freeze–thawed between liquid nitrogen and a 50 °C water bath for 10 times to form multilamellar vesicles (MLV). The 10 mol% POPG helped decreasing the large aggregates formed when pure POPE is dispersed in aqueous solution.[38] The acceptor MLV and the donor SUV dispersions were centrifuged at 20 000 × *g* for 30 min at 4 °C to remove small vesicles from the acceptor MLV and large vesicles from the donor SUV solutions. The remaining pellet for the acceptor MLVs and the SUV supernatant was kept.

The SUVs dispersion was diluted with aliquots of a 70 mM mβCD solution and mqH_2O to reach a final methyl-β-cyclodextrin (mβCD) concentration of 35 mM and a molar ratio of 8 : 1 mβCD to lipid. This dispersion was incubated for 2 h at 37 °C under magnetic stirring to preload the mβCD with donor lipids. After 2 h, the dispersion was used to dilute the MLV pellet at 2 : 1 donor : acceptor lipid molar ratio and incubated for 30 min at 37 °C under magnetic stirring to exchange the outer leaflet lipids on the MLV acceptor preparation. Subsequently, the samples were diluted with a 35 mM NaCl solution to 50 ml and transferred to 50 ml Falcon tubes, which were centrifuged at 20 000 × *g* for 30 min at 4 °C. The pellet including ∼0.5 ml of the remaining supernatant on the bottom of the tube was redissolved with mqH_2O containing 35 mM NaCl to a volume of 1 ml and transferred to 1.5 ml Eppendorf tubes. The tubes were centrifuged at 20 000 × *g* for 30 min at 4 °C to form a pellet. Finally, the lipid pellets were transferred into 4 mm MAS NMR rotors and immediately measured.

For symmetric control MLV samples, lipids were dissolved in 2 ml cyclohexane after solvent evaporation and lyophilized overnight to form a fluffy powder that is easy to hydrate. The powders were hydrated to 50 wt% using mqH_2O containing 35 mM NaCl and freeze–thawed between 50 °C water bath and LN_2 to form MLVs. Samples were transferred into 4 mm MAS NMR rotors and stored at −20 °C until measured.

2.2 Solid state NMR measurements

The samples were measured on a Bruker 750 Avance I NMR spectrometer using a resonance frequency of 115.1 MHz for ^{2}H. A 4 mm triple gradient MAS probe was used but without spinning to acquire static ^{2}H NMR spectra using a phase-cycled quadrupolar echo sequence[39] with a 30 μs delay between the two π/2 pulses of ∼3 μs length each. The spectral width was 500 kHz and the recycling delay 1 s. The order parameters[40] and chain extension profiles were calculated using Mathcad programs for dePakeing and previously described[41] methods using the mean torque model.[42] For measuring the T_{1Z} relaxation times an inversion recovery pulse sequence with quadrupole echo and a delay list of 0.001, 0.007, 0.015, 0.03, 0.07, 0.12, 0.18, 0.25, 0.5, 1, 2.5 s with a relaxation delay of 2.5 s was used. The R_{Z1} relaxation rates of the ^{2}H NMR powder spectra were calculated using a program written in Mathcad as previously described.[43] Briefly, the ^{2}H NMR line shapes were simulated using 15 Pake doublets and one isotropic peak for the asymmetric samples. From the fit of the inversion recovery data, the spin lattice relaxation time of each peak was determined.

2.3 Preparation of asymmetric LUV for testing lipid exchange efficiency

For the preparation of asymmetric LUVs, we followed the protocol of Doktorova *et al.*[10] without significant modifications. For both donor and acceptor vesicle

preparation, lipids were dissolved in $CHCl_3$/MeOH (1 : 1 v/v) and evaporated as above. Both acceptor and donor vesicles were dissolved in 35 mM NaCl H_2O to reach a concentration of 10 mg ml^{-1}. Donor MLVs were prepared from the respective lipid mixes by freeze thawing. Acceptor vesicles were prepared by extrusion using two 100 nm Teflon filters 25 times to obtain large unilamellar vesicles (LUV). The donor MLV dispersions were centrifuged at 20 000 × *g* for 30 min at 4 °C to separate the small vesicles from the donor MLV. The donor MLV pellet was dissolved and diluted in 70 mM mβCD solution and further diluted with mqH_2O to reach a final mβCD concentration of 35 mM (at an 8 : 1 mβCD to lipid molar ratio) and incubated at 37 °C for 2 h under magnetic stirring to preload the mβCD with donor lipids. After 2 h, the LUV acceptor solution was added at 2 : 1 donor : acceptor molar ratio incubated for 30 min at 37 °C under magnetic stirring for the exchange of the outer leaflet lipids on the LUV acceptor. Subsequently, the samples were diluted with 35 mM NaCl H_2O to 50 ml and transferred to a 50 ml Falcon tube and centrifuged at 20 000 × *g* for 30 min at 4 °C. The supernatant was carefully removed with a glass Pasteur pipet until ~2 ml of the pellet was left. To remove mβCD and mβCD–lipid complexes from the supernatant, Amicon® Ultra Filters (Merck KGaA, Darmstadt, Germany) with a 100 kDa MWCO were used in a swing bucket centrifuge (4000 × *g* at room temperature) until the volume was reduced to a few ml. Before use the centrifugation filters were wetted with 10 ml of mqH_2O and centrifuged at 4000 × *g* for 10 min at room temperature. Subsequently, the samples were extracted and lipid concentration was quantified using TLC.

2.4 Thin layer chromatography

The lipids from the LUV dispersions were extracted following the method described by Bligh and Dyer.[44] Specifically, 200 µl of the LUV dispersion were combined with 400 µl of $CHCl_3$/MeOH (1 : 1 [v/v]) in a glass vial and mixed for 30 s. A 5 min centrifugation step at 10 000 × *g* and 20 °C provided phase separation. The lipid-containing $CHCl_3$ phase was transferred to a clean glass vial and for the remaining aqueous phase, the procedure was repeated twice using 200 µl $CHCl_3$ for each step and organic phases were combined. $CHCl_3$ from the combined phases was evaporated using a vacuum rotation concentrator (RVC 2-25, Martin Christ Gefriertrocknungsanlagen GmbH, Osterode am Harz, Germany). The resulting lipid film was redissolved in 200 µl $CHCl_3$. Triplicates of the mixture were applied in 1.5, 2, 2.5 µl spots for POPS, POPC and POPE and in 6, 7, 8 µl spots for POPG to a high-performance thin-layer chromatography (HPTLC) silica gel 60 plate (Merck KGaA) by a CAMAG Linomat 5 sample applicator (CAMAG, Berlin, Germany). POPS, POPE, and POPC (0.5 mg ml^{-1} in $CHCl_3$) and POPG (1 mg ml^{-1} in $CHCl_3$) were applied as lipid calibration standards to the same HPTLC plate. Chromatographic separation was carried out in a CAMAG glass chamber using a mobile phase consisting of chloroform/ethanol/water/triethylamine (30 : 35 : 7 : 35 [v/v/v/v]) for 45 min.[45] Lipid spots were visualized by staining with primuline (Sigma-Aldrich, Taufkirchen, Germany), 100 mg l^{-1} in acetone/H_2O (4 : 1 [v/v]), followed by excitation at 366 nm. The picture was recorded in the black and white mode and the densitometric analysis (band volume) of each band was calculated using totallab quant 2.2 software (totallab, Newcastle, UK). The calibration curve was fitted with Origin software (version 9.60, Originlab corporation,

Northampton, MA, USA), using a single exponential model equation, from which the sample lipid concentrations were derived.

2.5 Matrix-assisted laser desorption/ionization time-of-flight mass spectrometry to detect mβCD

The asymmetric MLVs were analyzed by matrix-assisted laser desorption/ionization time-of-flight mass spectrometry (MALDI-TOF MS) to check for remaining mβCD. One μl of each sample (~5% of the sample) was filled to 10 μl with methanol and subsequently mixed with 10 μl of the respective matrix. DHB[46] (0.5 M in methanol) was used as the matrix to record mass spectra in the positive ion mode, 9-AA (10 mg ml^{-1} in 2-propanol/acetonitrile (3 : 2, v/v)) served as the matrix for negative ion spectra. The diluted asymmetric MLV samples were mixed 1 : 1 (v/v) with the respective matrix and vortexed for good homogeneity. Subsequently, 0.75 μl of the respective solution were transferred onto an aluminum-coated MALDI target (Bruker Daltonics GmbH, Bremen, Germany). Instantly after air drying, positive and negative ion mass spectra were recorded on an Autoflex Speed mass spectrometer (Bruker Daltonics) utilizing a Neodym-YAG laser emitting at 355 nm. The extraction voltage was 20 kV and gated matrix suppression was applied to prevent the saturation of the detector by matrix ions. For each mass spectrum, 10 000 single laser shots were averaged. The laser fluency was kept about 10% above threshold (*i.e.* the minimum laser fluency required to detect any signals) to obtain an optimum signal-to-noise ratio. All spectra were acquired in the reflector mode using delayed extraction conditions. Raw data were processed using the software "Flex Analysis" version 3.0 (Bruker Daltonics).

3 Results

We prepared two samples of asymmetric membranes. These systems consisted of POPE/POPG (molar ratio 9 : 1) multilamellar vesicles (MLVs) in which only the outer bilayer was prepared asymmetrically. To this end, SUVs of either POPC-d_{31} or POPS-d_{31}, both perdeuterated in the *sn*-1 chain, served as donor vesicles. After mβCD-catalyzed exchange, the MLVs were centrifuged and the pellet was used as sample for the ^{2}H NMR experiments. As control, we used four symmetric MLV preparations composed of POPC-d_{31}, POPS-d_{31}, POPC-d_{31}/POPE/POPG (molar ratio 10 : 9 : 1) and POPS-d_{31}/POPE/POPG (molar ratio 10 : 9 : 1). The lipid mixing ratio of the symmetric vesicles was chosen assuming that all lipids are homogeneously distributed between the two leaflets.

Typical ^{2}H solid-state NMR spectra are shown in Fig. 1. The NMR spectra of both pure POPC and POPS as well as the symmetric vesicles show powder patterns of well-resolved Pake doublets assignable to the individual methylene and methyl segments of the chain. The NMR spectra of the asymmetric membranes are characterized by a larger line width and an isotropic peak indicating somewhat slower motions (*i.e.* shorter T_2 times) and a minor fraction (~7–9%) of lipids in highly curved geometry.

In the series where deuterated POPC-d_{31} was used, pure POPC gives the narrowest spectrum. Both the symmetric and the asymmetric membranes provide broader ^{2}H NMR spectra, indicating higher chain order parameters. In contrast,

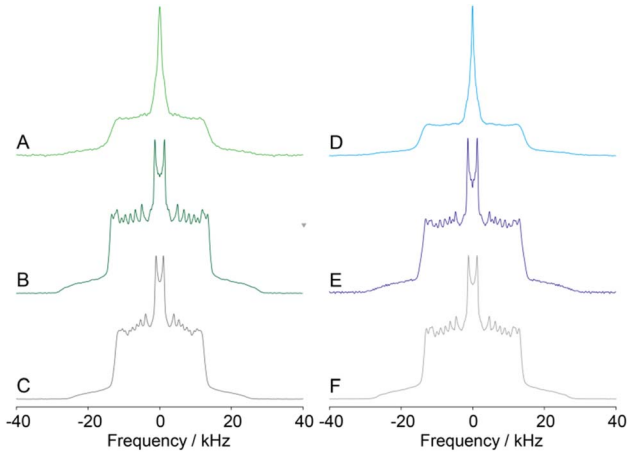

Fig. 1 Solid-state ^{2}H NMR spectra of multilamellar vesicle preparations with symmetric and asymmetric lipid distribution. (Left) ^{2}H NMR spectra of asymmetric POPC-d_{31}^{out}/(POPE/POPG)^{in} membranes (A), symmetric POPC-d_{31}/POPE/POPG bilayers (B), and pure POPC-d_{31} membranes (C). (Right) ^{2}H NMR spectra of asymmetric POPS-d_{31}^{out}/(POPE/POPG)^{in} membranes (D), symmetric POPS-d_{31}/POPE/POPG bilayers (E), and pure POPS-d_{31} membranes (F).

the NMR spectra of the POPS-d_{31}-containing samples are of relatively similar width. These differences can be discussed more quantitatively after dePakeing of the spectra and calculating the order parameters (S) along the chains for all samples.

Fig. 2A compares the order parameters (S) of the POPC-d_{31}-containing samples. For pure POPC, the typical order parameter plateau of the upper chain and the strongly decreasing order parameters in the lower chain are observed. The symmetric POPC-d_{31}/POPE/POPG membranes show the same features, but for the entire chain, the order parameters are about 10–20% larger. This is caused by the presence of POPE, which is characterized by a negative intrinsic curvature that induces tighter lipid packing in PE-containing mixtures.[8,47] The order parameters

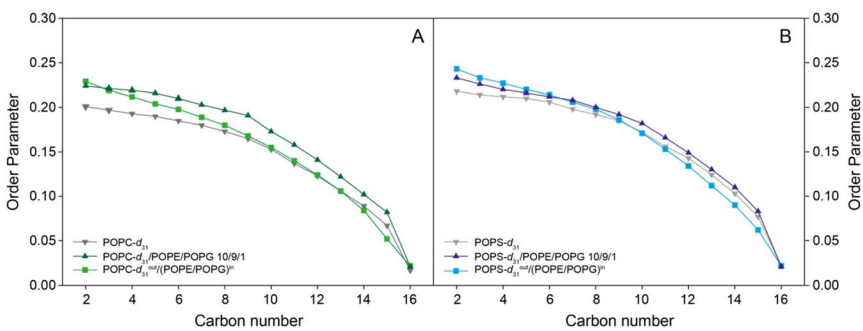

Fig. 2 Smoothed ^{2}H NMR order parameter plots of symmetric and asymmetric MLVs determined from the ^{2}H NMR spectra shown in Fig. 1. (A) Order parameters of POPC-d_{31} and (B) order parameters of POPS-d_{31} are plotted. The temperature of the measurement was 37 °C.

of the asymmetric POPC^{out}/(POPE/POPG)^{in} membranes show a distinctly different shape. While the upper ~3 carbons show slightly higher or similar order as the POPC in symmetric membranes, order parameters drop rather steeply, fall even below those of pure POPC starting at carbon position 8, and remain lower for the entire lower chain. Such a behavior of the chain order parameters has for instance been observed for the lipid modifications of Ras proteins that were inserted into membranes of lower hydrophobic thickness than the length of the Ras lipid modification.[48]

In Fig. 2B, the order parameters of pure POPS-d_{31}, symmetric POPS-d_{31}/POPE/POPG, and asymmetric POPS-d_{31}^{out}/(POPE/POPG)^{in} are compared. PS membranes are also characterized by higher order parameters than observed for PC bilayers.[47] Therefore, the addition of POPE as in the symmetric POPS-d_{31}/POPE/POPG bilayers does not lead to a very significant increase in chain order. In the asymmetric POPS^{out}/(POPE/POPG)^{in}, we observe a similar tendency as seen for asymmetric POPC^{out}/(POPE/POPG)^{in} bilayers: the upper chain segments of the POPS chain show higher order parameters, while the lower segments are characterized by lower order compared to pure POPS and the symmetric POPS-d_{31}/POPE/POPG bilayers.

The differences in the order parameters are also reflected in the length of the lipid's acyl chains, where lower order generally corresponds to shorter projected chain lengths.[42,49] We calculated these geometric parameters for the lipid's acyl chains using Brown's mean torque model.[42] For pure POPC, we measure an average chain length of 12.6 Å in agreement with previous data.[50] Due to the presence of POPE that is characterized by a high negative intrinsic curvature as discussed above, chain length of POPC in the presence of POPE increases to 13.3 Å. Interestingly, the chain length of the POPC in the outer leaflet of the asymmetric membranes is found to be 12.7 Å, which corresponds well to the pure POPC membranes.

For POPS, we had seen relatively similar order parameter profiles and the chain lengths calculated are also very similar (13.2 Å for pure POPS), 13.3 Å for symmetric POPS/POPE/POPG membranes, and 13.2 Å for asymmetric POPS^{out}/(POPE/POPG)^{in} membranes. This is also reflected in the chain extension plots, which are shown in ESI Fig. S1.†

Obviously, the packing and dynamic properties of POPC and POPS in asymmetric membranes are quite different from symmetric bilayers. To further characterize the elastic properties of the asymmetric preparations, we measured ^{2}H T_{1Z} relaxation times and plotted the relaxation rate R_{1Z} as a function of the square of the order parameter (S^2) for each lipid segment. These "square law plots" have empirically been shown to describe the elastic properties of membranes.[51–53] For saturated lipid membranes, a straight line is observed suggesting a $R_{1Z} \propto S^2$ proportionality.[51–53] In the presence of detergents, which make membranes softer, the R_{1Z} *vs.* S^2 plot is curved and characterized by a steeper slope and a $R_{1Z} \propto S^n$ proportionality where $n < 2$.[51] Such behavior has also been observed for mono-unsaturated lipids as POPC.[54] In the presence of cholesterol, which makes membranes stiffer, the slope of the R_{1Z} *vs.* S^2 plot is shallower but linear. These plots represent a useful measure for a qualitative evaluation of the membrane's elastic properties. Alterations in membrane structure that lead to a rigidization are accompanied by a decrease in the slope of the R_{1Z} *vs.* S^2 plot; alterations that

make membranes more elastic are manifested in a convexly shaped curve in the R_{1Z} *vs.* $S^{n<2}$ plot with a steeper slope.

Fig. 3 shows these square law plots for both asymmetric membrane preparations and the respective controls. For pure POPC-d_{31} MLVs, a similar plot is observed as reported before.[54] The data can be fitted with the function $R_{1Z} = y_0 + a \times S^n$, where n should be 2 in an ideal square law plot. For the pure POPC membranes, we determined $n = 1.02$, indicating a significant deviation from the square law in agreement with soft POPC membranes characterized by a $R_{1Z} \propto \sqrt{S^2}$ proportionality. For the symmetric POPC-d_{31}/POPE/POPG membranes, the plot becomes shallower and the exponent determined from the fit increased to $n = 1.52$. For the asymmetric POPC^{out}/(POPE/POPG)^{in} membranes, the exponent further increased to $n = 1.62$.

The empiric relation between R_{1Z} and S^2 can be used to compare the elastic properties of the different membranes. Monounsaturated membranes are generally more elastic than saturated ones, which leads to a convexly curved R_{1Z} *vs.* S^2 plot. Mathematically, this is manifested by a $R_{1Z} \propto S^n$ plot, where $n < 2$. If the

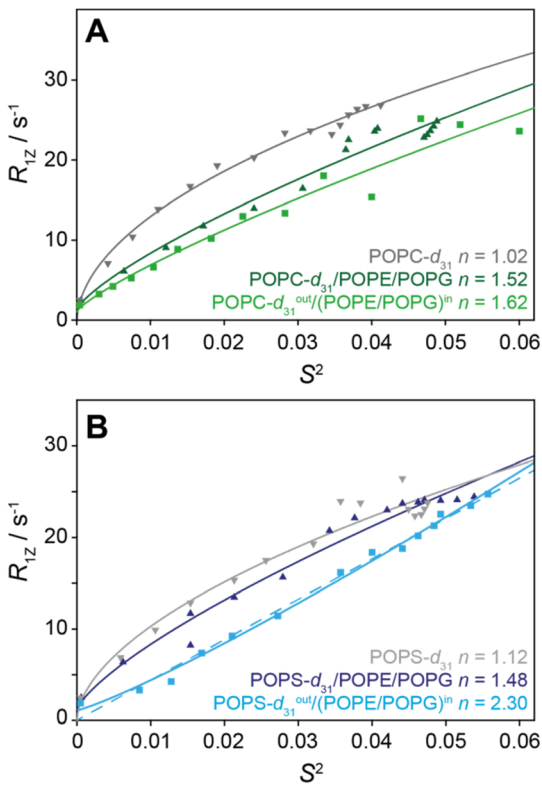

Fig. 3 (A) Square law plots of POPC-d_{31}^{out}/(POPE/POPG)^{in} membranes (light green squares), symmetric POPC-d_{31}/POPE/POPG bilayers (dark green triangles), and pure POPC-d_{31} membranes (gray upside down triangles). (B) Square law plots of POPS-d_{31}^{out}/(POPE/POPG)^{in} membranes (light blue squares), symmetric POPS-d_{31}/POPE/POPG bilayers (dark blue triangles), and pure POPS-d_{31} membranes (light gray upside down triangles). The lines represent best fits to the function $R_{1Z} = y_0 + a \times S^n$, and the dashed solid line represents a linear regression.

membrane becomes more rigid, n also increases, which is what is observed here; n increases from 1.02 for pure POPC membranes to 1.52 for symmetric and 1.62 to asymmetric bilayers. This suggests that the symmetric POPC-d_{31}/POPE/POPG membranes are more rigid than pure POPC, which is explained by the high negative intrinsic curvature of POPE. The outer leaflet of asymmetric POPC^{out}/(POPE/POPG)^{in} is slightly more rigid, although it is composed of a relatively pure POPC layer. This suggests that the higher rigidity of the inner PE-containing leaflet dominates the elastic properties of the entire membrane.

An important parameter for discussing this interesting behavior is the efficiency of the lipid exchange of the outer leaflet of the MLVs. For instance, if the outer layer still contained a high proportion of POPE, the difference in the R_{1Z} *vs.* S^2 plots of pure POPC and asymmetric POPC^{out}/(POPE/POPG)^{in} membranes could be explained by the presence of POPE, which has a negative intrinsic curvature. Lipid analysis of the MLVs, where only the outer leaflet was exchanged, is difficult as all lipids of the inner (symmetric) layers are also measured. Therefore, we prepared POPE/POPG (molar ratio 9 : 1) LUVs and exchanged the outer layer with POPC-d_{31} using a similar procedure as for the asymmetric MLVs. By quantitative thin layer chromatography (ESI Fig. S2†), we determined the amount of POPC to be 48.7% and the POPE to be 51.3%. For this preparation, the POPG spot was too weak for quantification. This suggests that the exchange of the outer layer was almost complete. For comparison, we analysed the symmetric POPC-d_{31}/POPE/POPG membranes and determined a molar lipid ratio of 50.3% POPC, 46.0% POPE, and 3.7% POPG, which is very close to the original mixing ratio. We also performed MALDI-TOF mass spectrometry to check for remaining mβCD in the MLV samples used for ^{2}H NMR (ESI Fig. S3†). Although quantification of the mass spectra is not possible, residual mβCD was clearly identified.

Next, we measured the relaxation rates for pure POPS-d_{31} membranes and plot them as a function of S^2 (Fig. 3B). Again, a curved plot is obtained that can be fitted with an exponent of $n = 1.12$. For the symmetric POPS-d_{31}/POPE/POPG membranes, the plot is similar but has a slightly higher exponent of $n = 1.48$ most likely because of the presence of POPE. For the asymmetric POPS^{out}/(POPE/POPG)^{in} membranes, an almost perfectly linear square law plot is obtained (dashed line). However, using the same fit function as above, an exponent of $n =$ 2.30 is found.

Finally, we also determined the relative composition of asymmetric LUVs and the symmetric preparations using TLC (ESI Fig. S2†). For the asymmetric POPS^{out}/(POPE/POPG)^{in} LUVs, we measured 65.9% POPS, 30.5% POPE, and 3.6% POPG, and for the symmetric POPE/POPG/POPS membranes, the ratio between the three lipids was 74% POPS, 24.4% POPE, and 1.6% POPG. The MALDI-TOF spectra of the preparations also showed remaining mβCD (ESI Fig. S3†).

4 Discussion

Asymmetric plasma membranes are a unique feature of pro- and eukaryotic organisms. As maintaining a broad lipid variety and the asymmetry between the two membrane leaflets consumes a considerable amount of energy, it is obvious that such a high effort is only maintained if absolutely required. Yet, our understanding of this intriguing biological situation is in its infancy. Now that robust procedures have been developed to prepare and characterize such

systems,[10] biophysical studies of the properties of asymmetric membranes and the impact on biological questions such as permeation, protein function, fusion, or lateral domain formation can be addressed.

Here, we discuss two asymmetric membrane preparations in comparison to symmetric bilayers. The first represents a model for the plasma membrane of mammalian cells with phosphatidylcholine in the outer and phosphatidylethanolamine and a negative lipid (here phosphatidylglycerol) in the inner leaflet. A methodological reason to use a small fraction of POPG was because pure POPE MLVs produce too large aggregates that are difficult to handle, which is remedied by 10 mol% POPG, which makes the MLV slightly smaller and prevents sedimentation of the acceptor vesicles. In the other system, the acidic lipid phosphatidylserine is in the outer leaflet, which is rather artificial as PS is normally found in the cytoplasmic leaflet unless cells undergo apoptosis.[55] Our choice of system is limited by the fact that for ^{2}H solid-state NMR applications, multilamellar vesicles need to be prepared as anisotropic NMR interactions that provide the structural and dynamic information are largely averaged in LUV systems.[56] This comes with the disadvantage that in an MLV system, we can exchange only the very outer leaflet of the vesicle, here by deuterated lipids, providing a unique probe to selectively detect the lipids in the outer leaflet. The drawback of this procedure is that the lipids that are naturally found in the cytoplasmic leaflet are not accessible in this preparation. But the outer bilayer of a MLV is a very good model for the plasma membrane as its dimensions compare much better to a cell than the LUVs.

A first question that we studied concerns the completeness of the lipid exchange. Given the characteristics of the MLV system, a quantitative measurement of the composition of the outer layer is difficult because the inner bilayers of the MLVs are symmetric and not accessible by the mβCD-catalyzed exchange. Therefore, we prepared LUVs by extrusion and exchanged the outer leaflet using the same strategy as in the MLV preparation. In the POPC^{out}/(POPE/POPG)^{in} LUVs, we found complete exchange of POPE/POPG with POPC rendering the resulting outer membrane of the MLVs completely asymmetric. In the POPS^{out}/(POPE/POPG)^{in} LUVs, we measured a slightly higher amount of POPS than what could be accommodated in the outer leaflet. It is not clear at this point if PS would possibly be subject to faster flip flop or if the cyclodextrin exchange could have resulted in a higher deposition of PS also in the inner leaflet. Another study also found donor lipids in the inner leaflet that should not have exchanged.[11] Nevertheless, it is quite obvious that highly asymmetric membranes were prepared and we assume that the exchange procedure was equally successful for the outer leaflet of the two MLV systems. We also checked if the NMR samples contained remaining mβCD and found the sugar to be present in both preparations, but a quantification of the mass spectra was not possible. If remaining mβCD may have an influence on the membrane is not clear at this point.

Our study shows that the order parameter profiles of the lipid molecules in symmetric and asymmetric membranes are different. In comparison to symmetric membranes, we find that lipid chain order is higher in the upper and lower in the lower half of the acyl chains for both POPC and POPS when exclusively located in the outer layer. This indicates different packing constraints in the asymmetric membranes. Remarkably, the acyl chain lengths of POPC in the outer leaflet only or in symmetric vesicles were identical within experimental error

(±0.1 Å); the same is observed for POPS, where the chain lengths are identical in both preparations. This supports the results from lipid analytics, which revealed that our preparations showed a very high degree of asymmetry. If POPE was prominently found in the outer leaflet, it would have increased the chain lengths in the outer leaflet. More interestingly, there seems to be a preference for higher order in the upper and lower order in the lower acyl chain when membranes show an asymmetric lipid distribution. This could possibly indicate an increased negative intrinsic curvature in the outer leaflet of asymmetric membranes. Such a steeper decrease in order along the acyl chains will likely modify the properties of the lipid/water interface and potentially alter the partitioning of small molecules, drugs, or peptides. MD simulations have also identified chain order parameter changes and altered lateral stress profiles between the leaflets in asymmetric membranes.[14,57] While the MD of asymmetric DPPC/DPPS membranes revealed a decrease in PC order and an increase in PS order when making membranes asymmetric,[14] our ^{2}H NMR results indicated a distinctly different chain order parameter profile.

From this, one may speculate about the mechanism of interleaflet coupling. The most invoked mechanism for this phenomenon is acyl chain interdigitation. For the two asymmetric systems (POPC^{out}/(POPE/POPG)^{in} and POPS^{out}/(POPE/POPG)^{in}), there is no neutron scattering data available that would most directly detect possible acyl chain interdigitation. ^{2}H NMR spectra and order parameters can also indicate chain interdigitation, although very clear information has only been obtained for lipids with large differences in acyl chain lengths.[58,59] The order parameters measured for the two systems studied here do not suggest acyl chain interdigitation, but it cannot safely be excluded either. Supportive of this notion is the systematic study by Frewein *et al.*,[15] showing that interdigitation was not observed if POPC was used as donor lipid (with DPPC on the inner membrane leaflet) but only for systems with a larger *sn*-1/*sn*-2 chain length difference. Altogether, it is fair to say that acyl chain interdigitation is unlikely to occur in the two systems.

Even though chain interdigitation is unlikely, the two membrane leaflets are not uncoupled from one another. Clearly, the inner membrane leaflet influenced the order parameters and elastic properties of the outer leaflet. An obvious difference between outer and inner leaflet is in lipid packing density. As the inner leaflet is rich in POPE, which is known for its negative intrinsic curvature, one could assume that the tighter packing of the inner leaflet is transmitted into the outer leaflet. One can speculate that these packing density alterations may very well be transmitted from one leaflet to the other. But with the current very limited data set, such conclusions remain fairly speculative.

We turned our attention to dynamic aspects of the lipids in the outer membrane leaflet. NMR relaxation rates are great parameters to study the molecular motions of the lipids in detail.[24,60] From first inspection of the ^{2}H NMR spectra of asymmetric membranes, it is clear that the line widths of the individual Pake doublets is increased, which indicates shorter T_2 values usually associated with slower lipid motions. Very straightforward is the measurement of ^{2}H T_{1Z} relaxation times of the deuterated chains. Relaxation rates ($R_{1Z} = 1/T_{1Z}$) decrease for asymmetric membranes compared to pure or symmetric preparations. A very convenient way of addressing the dynamic behavior of lipid membranes and assess their elastic properties are the square law plots, where R_{1Z} is plotted against

the square of the order parameter (S^2) of the respective segment.[60] In the pioneering work from the Brown laboratory, a square law dependence ($R_{1Z} \propto S^2$) was obtained for saturated (symmetric) membranes of varying chain lengths,[60] which is interpreted as a dominant contribution of low frequency motions in agreement with a collective model for slow motions on the mesoscopic scale (1–100 nm). In the presence of cholesterol, which makes membranes stiffer, R_{1Z} is still proportional to S^2, but the slope of the curves decreases with increasing cholesterol content.[61] In the presence of detergents, such as $C_{12}E_8$,[51] unsaturated lipid chains,[62,63] or the lipid modifications of a lipidated peptide[48] are found to follow a $R_{1Z} \propto S^n$ proportionality, where $n < 2$ and in some cases even a linear $R_{1Z} \propto S$ relationship has been observed.[54]

Here, we found rather strong deviations from the $n = 2$ power law as expected for monounsaturated membranes in agreement with relatively soft lipid membranes.[54] Pure POPC or POPS membranes showed highest elasticity, while the addition of POPE in symmetric membranes slightly rigidified the membranes. Plotting R_{1Z} *vs.* S^2 for the outer leaflet of POPC^{out}/(POPE/POPG)^{in} and POPS^{out}/(POPE/POPG)^{in} revealed an additional increase in stiffness where especially the POPS-rich leaflet behaved quite like a fully saturated membrane. These results are in agreement with studies that observed that cholesterol-free asymmetric bilayers feature increased bending rigidities.[12,29,64] However, the increased bending rigidity of asymmetric membranes has been discussed in relation to the enrichment of saturated sphingolipids and cholesterol in the outer and (poly-)unsaturated lipids in the inner leaflet. Here, all the membranes were composed of monounsaturated lipids only. It is well known that POPE increases the packing density of membranes leading to increased stiffness.[25] In agreement with our results, Frewein *et al.*[15] also observed an increase in bending rigidity in asymmetric POPC^{out}/POPE^{in} bilayers compared to scrambled POPC/POPE membranes. This clearly indicates that the higher bending rigidity of the inner POPC layer dominates the elastic properties of the asymmetric membranes. This, along with the other recent results on asymmetric membranes, provides an imperative to consider leaflet asymmetry as a crucial determinant of membrane properties and likely protein functions as shown in first studies.

5 Conclusions

We investigated biophysical properties of lipid membranes with leaflet asymmetry in the distribution of lipid species featuring POPE/POPG (9 : 1) lipids in the inner and either POPC or POPS in the outer leaflet. ^{2}H NMR chain order parameters revealed an intriguing reshuffling of order from the lower to the upper chain segments of the outer leaflet of asymmetric compared to symmetric membranes. Interestingly, the overall chain lengths remained constant compared to symmetric bilayers of the same lipid species. This suggests that the lateral stress and lateral pressure profile of asymmetric bilayers is considerably different, leading to alteration in the lipid–protein interactions with likely consequences for protein function. This is also implied from the increase in stiffness of asymmetric membranes differing in the headgroup but not in the chain composition. An interleaflet coupling is the likely mechanism for this interesting behavior, but from the results of this work, no indications for interdigitation of the acyl chains between the lipids of the individual leaflets could be observed. One could

speculate that the packing density of one leaflet is sensed by the other and that these parameters are correlated between the leaflets. This would suggest that lipid dynamics is also correlated between the molecules of the two leaflets. While the tools to investigate such correlations in lipid dynamics within specific correlation time windows have been developed,[24,65] a current limitation for NMR applications is the necessity to rely on anisotropic NMR interactions that are largely averaged in unilamellar vesicles. But solutions to this problem are underway, which will allow also detecting NMR parameters of the lipids in the inner leaflet.

Data availability

Tables with all order parameters and R_{1Z} relaxation rates for the various membrane preparations determined from the experimental NMR spectra are available in the supplementary information file.†

Author contributions

D. H. designed the study. O. E. made all sample preparations, and carried out the NMR experiments. O. E. and D. H. analysed the ^{2}H NMR spectra. V. D. determined the lipid concentration. K. M. E. carried out the mass spectrometry and analyzed the data. D. H. and O. E. wrote the paper with contributions from all coauthors.

Conflicts of interest

There are no conflicts to declare.

Acknowledgements

The study was funded by the Deutsche Forschungsgemeinschaft (DFG, German Research Foundation), project numbers 546534953 and 511424302.

References

1 J. H. Lorent, K. R. Levental, L. Ganesan, G. Rivera-Longsworth, E. Sezgin, M. Doktorova, E. Lyman and I. Levental, Plasma membranes are asymmetric in lipid unsaturation, packing and protein shape, *Nat. Chem. Biol.*, 2020, **16**, 644–652.
2 G. van Meer, D. R. Voelker and G. W. Feigenson, Membrane lipids: where they are and how they behave, *Nat. Rev. Mol. Cell Biol.*, 2008, **9**, 112–124.
3 B. J. Litman and D. C. Mitchell, A role for phospholipid polyunsaturation in modulating membrane protein function, *Lipids*, 1996, **31**, 193–197.
4 M. Liscovitch and L. C. Cantley, Lipid second messengers, *Cell*, 1994, **77**, 329–334.
5 R. Baccouch, E. Rascol, K. Stoklosa and I. D. Alves, The role of the lipid environment in the activity of G protein coupled receptors, *Biophys. Chem.*, 2022, **285**, 106794.
6 N. Thakur, A. P. Ray, L. Sharp, B. Jin, A. Duong, N. G. Pour, S. Obeng, A. V. Wijesekara, Z. G. Gao, C. R. McCurdy, K. A. Jacobson, E. Lyman and

M. T. Eddy, Anionic phospholipids control mechanisms of GPCR-G protein recognition, *Nat. Commun.*, 2023, **14**, 794.

7 M. Damian, M. Louet, A. A. S. Gomes, C. M'Kadmi, S. Denoyelle, S. Cantel, S. Mary, P. M. Bisch, J. A. Fehrentz, L. J. Catoire, N. Floquet and J.-L. Banères, Allosteric modulation of ghrelin receptor signaling by lipids, *Nat. Commun.*, 2021, **12**, 3938.

8 O. Engberg, D. Ulbricht, V. Dobel, V. Siebert, C. Frie, A. Penk, M. K. Lemberg and D. Huster, Rhomboid-catalyzed intramembrane proteolysis requires hydrophobic matching with the surrounding lipid bilayer, *Sci. Adv.*, 2022, **8**, eabq8303.

9 G. Pabst and S. Keller, Exploring membrane asymmetry and its effects on membrane proteins, *Trends Biochem. Sci.*, 2024, **49**, 333–345.

10 M. Doktorova, F. A. Heberle, B. Eicher, R. F. Standaert, J. Katsaras, E. London, G. Pabst and D. Marquardt, Preparation of asymmetric phospholipid vesicles for use as cell membrane models, *Nat. Protoc.*, 2018, **13**, 2086–2101.

11 B. Eicher, D. Marquardt, F. A. Heberle, I. Letofsky-Papst, G. N. Rechberger, M. S. Appavou, J. Katsaras and G. Pabst, Intrinsic curvature-mediated transbilayer coupling in asymmetric lipid vesicles, *Biophys. J.*, 2018, **114**, 146–157.

12 M. P. K. Frewein, P. Piller, E. F. Semeraro, O. Czakkel, Y. Gerelli, L. Porcar and G. Pabst, Distributing aminophospholipids asymmetrically across leaflets causes anomalous membrane stiffening, *Biophys. J.*, 2023, **122**, 2445–2455.

13 P. Piller, E. F. Semeraro, G. N. Rechberger, S. Keller and G. Pabst, Allosteric modulation of integral protein activity by differential stress in asymmetric membranes, *PNAS Nexus*, 2023, **2**, pgad126.

14 L. Pasalic, P. Males, A. Cikos, B. Pem and D. Bakaric, The rise of FTIR spectroscopy in the characterization of asymmetric lipid membranes, *Spectrochim. Acta, Part A*, 2024, **305**, 123488.

15 M. P. K. Frewein, P. Piller, E. F. Semeraro, K. C. Batchu, F. A. Heberle, H. L. Scott, Y. Gerelli, L. Porcar and G. Pabst, Interdigitation-induced order and disorder in asymmetric membranes, *J. Membr. Biol.*, 2022, **255**, 407–421.

16 M. Doktorova, J. L. Symons, X. Zhang, H.-Y. Wang, J. Schlegel, J. H. Lorent, F. A. Heberle, E. Sezgin, E. Lyman, K. R. Levental and I. Levental, Cell membranes sustain phospholipid imbalance *via* cholesterol asymmetry, *bioRxiv*, 2024, preprint, DOI: **10.1101/2023.07.30.551157**.

17 Y. Zhu, L. Porcar, T. Ravula, K. C. Batchu, T. L. Lavoie, Y. Liu and U. Perez-Salas, Unexpected asymmetric distribution of cholesterol and phospholipids in equilibrium model membranes, *Biophys. J.*, 2024, **123**, 3923–3934.

18 Q. Lin and E. London, The influence of natural lipid asymmetry upon the conformation of a membrane-inserted protein (perfringolysin O), *J. Biol. Chem.*, 2014, **289**, 5467–5478.

19 E. Perozo, A. Kloda, D. M. Cortes and B. Martinac, Physical principles underlying the transduction of bilayer deformation forces during mechanosensitive channel gating, *Nat. Struct. Biol.*, 2002, **9**, 696–703.

20 H. I. Petrache, N. Gouliaev, S. Tristram-Nagle, R. Zhang, R. M. Suter and J. F. Nagle, Interbilayer interactions from high resolution x-ray scattering, *Phys. Rev. E: Stat. Phys., Plasmas, Fluids, Relat. Interdiscip. Top.*, 1998, **57**, 7014–7024.

21 M. C. Wiener and S. H. White, Structure of a fluid dioleoylphosphatidylcholine bilayer determined by joint refinement of x-ray and neutron diffraction data III. Complete structure, *Biophys. J.*, 1992, **61**, 434–447.
22 S. L. Veatch, O. Soubias, S. L. Keller and K. Gawrisch, Critical fluctuations in domain-forming lipid mixtures, *Proc. Natl. Acad. Sci. U. S. A.*, 2007, **104**, 17650–17655.
23 D. Huster, K. Arnold and K. Gawrisch, Investigation of lipid organization in biological membranes by two-dimensional nuclear Overhauser enhancement spectroscopy, *J. Phys. Chem. B*, 1999, **103**, 243–251.
24 A. A. Smith, A. Vogel, O. Engberg, P. W. Hildebrand and D. Huster, A method to construct the dynamic landscape of a bio-membrane with experiment and simulation, *Nat. Commun.*, 2022, **13**, 108.
25 A. V. Botelho, N. J. Gibson, R. L. Thurmond, Y. Wang and M. F. Brown, Conformational energetics of rhodopsin modulated by nonlamellar-forming lipids, *Biochemistry*, 2002, **41**, 6354–6368.
26 M. F. Brown, Soft matter in lipid-protein interactions, *Annu. Rev. Biophys.*, 2017, **46**, 379–410.
27 W. E. Teague, O. Soubias, H. Petrache, N. Fuller, K. G. Hines, R. P. Rand and K. Gawrisch, Elastic properties of polyunsaturated phosphatidylethanolamines influence rhodopsin function, *Faraday Discuss.*, 2013, **161**, 383–395.
28 O. Soubias, W. E. Teague Jr, K. G. Hines, D. C. Mitchell and K. Gawrisch, Contribution of membrane elastic energy to rhodopsin function, *Biophys. J.*, 2010, **99**, 817–824.
29 B. W. Rickeard, M. H. L. Nguyen, M. DiPasquale, C. G. Yip, H. Baker, F. A. Heberle, X. B. Zuo, E. G. Kelley, M. Nagao and D. Marquardt, Transverse lipid organization dictates bending fluctuations in model plasma membranes, *Nanoscale*, 2020, **12**, 1438–1447.
30 C. M. Brown and S. J. Marrink, Modeling membranes in situ, *Curr. Opin. Struct. Biol.*, 2024, **87**, 102837.
31 M. D. Weiner and G. W. Feigenson, Molecular dynamics simulations reveal leaflet coupling in compositionally asymmetric phase-separated lipid membranes, *J. Phys. Chem. B*, 2019, **123**, 3968–3975.
32 R. Vacha, M. L. Berkowitz and P. Jungwirth, Molecular model of a cell plasma membrane with an asymmetric multicomponent composition: water permeation and ion effects, *Biophys. J.*, 2009, **96**, 4493–4501.
33 E. H. Chaisson, F. A. Heberle and M. Doktorova, Building asymmetric lipid bilayers for molecular dynamics simulations: what methods exist and how to choose one?, *Membranes*, 2023, **13**, 629.
34 D. Huster, S. Maiti and A. Herrmann, Phospholipid membranes as chemically and functionally tunable materials, *Adv. Mater.*, 2024, **36**, e2312898.
35 F. A. Heberle, D. Marquardt, M. Doktorova, B. Geier, R. F. Standaert, P. Heftberger, B. Kollmitzer, J. D. Nickels, R. A. Dick, G. W. Feigenson, J. Katsaras, E. London and G. Pabst, Subnanometer structure of an asymmetric model membrane: interleaflet coupling influences domain properties, *Langmuir*, 2016, **32**, 5195–5200.
36 D. Marquardt, F. A. Heberle, T. Miti, B. Eicher, E. London, J. Katsaras and G. Pabst, ^{1}H NMR Shows Slow Phospholipid Flip-Flop in Gel and Fluid Bilayers, *Langmuir*, 2017, **33**, 3731–3741.

37 V. V. Kumar and W. J. Baumann, Bilayer asymmetry in lysophosphatidylcholine/cholesterol (1:1) vesicles. A phosphorus-31 NMR study, *Biochem. Biophys. Res. Commun.*, 1986, **139**, 25–30.
38 N. Kucerka, J. Pencer, J. N. Sachs, J. F. Nagle and J. Katsaras, Curvature effect on the structure of phospholipid bilayers, *Langmuir*, 2007, **23**, 1292–1299.
39 J. H. Davis, K. R. Jeffrey, M. Bloom, M. I. Valic and T. P. Higgs, Quadrupolar echo deuteron magnetic resonance spectroscopy in ordered hydrocarbon chains, *Chem. Phys. Lett.*, 1976, **42**, 390–394.
40 M. Lafleur, B. Fine, E. Sternin, P. R. Cullis and M. Bloom, Smoothed orientational order profile of lipid bilayers by ^{2}H-nuclear magnetic resonance, *Biophys. J.*, 1989, **56**, 1037–1041.
41 D. Huster, K. Arnold and K. Gawrisch, Influence of docosahexaenoic acid and cholesterol on lateral lipid organization in phospholipid membranes, *Biochemistry*, 1998, **37**, 17299–17308.
42 H. I. Petrache, S. W. Dodd and M. F. Brown, Area per lipid and acyl length distributions in fluid phosphatidylcholines determined by ^{2}H NMR spectroscopy, *Biophys. J.*, 2000, **79**, 3172–3192.
43 A. Vogel, K.-T. Tan, H. Waldmann, S. E. Feller, M. F. Brown and D. Huster, Flexibility of ras lipid modifications studied by ^{2}H solid-state NMR and molecular dynamics simulations, *Biophys. J.*, 2007, **93**, 2697–2712.
44 E. G. Bligh and W. J. Dyer, A rapid method of total lipid extraction and purification, *Can. J. Biochem. Physiol.*, 1959, **37**, 911–917.
45 M. Leopold, P. B. Mass-Sanchez, M. Krizanac, P. Stancl, R. Karlic, P. Prabutzki, V. Parafianczuk, J. Schiller, A. Asimakopoulos, K. M. Engel and R. Weiskirchen, How the liver transcriptome and lipid composition influence the progression of nonalcoholic fatty liver disease to hepatocellular carcinoma in a murine model, *Biochim. Biophys. Acta*, 2025, **1870**, 159574.
46 J. Schiller, J. Arnhold, S. Benard, M. Müller, S. Reichl and K. Arnold, Lipid analysis by matrix-assisted laser desorption and ionization mass spectrometry: a methodological approach, *Anal. Biochem.*, 1999, **267**, 46–56.
47 D. Huster, K. Arnold and K. Gawrisch, Strength of Ca^{2+} binding to retinal lipid membranes: consequences for lipid organization, *Biophys. J.*, 2000, **78**, 3011–3018.
48 A. Vogel, C. P. Katzka, H. Waldmann, K. Arnold, M. F. Brown and D. Huster, Lipid modifications of a ras peptide exhibit altered packing and mobility *versus* host membrane as detected by ^{2}H solid-state NMR, *J. Am. Chem. Soc.*, 2005, **127**, 12263–12272.
49 J. F. Nagle, Area/lipid of bilayers from NMR, *Biophys. J.*, 1993, **64**, 1476–1481.
50 T. Meyer, D. J. Baek, R. Bittman, I. Haralampiev, P. Muller, A. Herrmann, D. Huster and H. A. Scheidt, Membrane properties of cholesterol analogs with an unbranched aliphatic side chain, *Chem. Phys. Lipids*, 2014, **184**, 1–6.
51 D. Otten, M. F. Brown and K. Beyer, Softening of membrane bilayers by detergents elucidated by deuterium NMR spectroscopy, *J. Phys. Chem. B*, 2000, **104**, 12119–12129.
52 M. F. Brown, R. L. Thurmond, S. W. Dodd, D. Otten and K. Beyer, Composite membrane deformation on the mesoscopic length scale, *Phys. Rev. E: Stat. Phys., Plasmas, Fluids, Relat. Interdiscip. Top.*, 2001, **64**, 010901.

53 M. F. Brown, R. L. Thurmond, S. W. Dodd, D. Otten and K. Beyer, Elastic deformation of membrane bilayers probed by deuterium NMR relaxation, *J. Am. Chem. Soc.*, 2002, **124**, 8471–8484.
54 H. A. Scheidt, R. M. Badeau and D. Huster, Investigating the membrane orientation and transversal distribution of 17β-estradiol in lipid membranes by solid-state NMR, *Chem. Phys. Lipids*, 2010, **163**, 356–361.
55 S. Nagata, Apoptosis and clearance of apoptotic cells, *Annu. Rev. Immunol.*, 2018, **36**, 489–517.
56 D. B. Fenske and P. R. Cullis, Acyl chain orientational order in large unilamellar vesicles: comparison with multilamellar liposomes: a ^{2}H and ^{31}P nuclear magnetic resonance study, *Biophys. J.*, 1993, **64**, 1482–1491.
57 T. L. Mai, P. Derreumaux and P. H. Nguyen, Structure and elasticity of mitochondrial membranes: a molecular dynamics simulation study, *J. Phys. Chem. B*, 2023, **127**, 10778–10791.
58 R. N. Lewis, R. N. McElhaney, M. A. Monck and P. R. Cullis, Studies of highly asymmetric mixed-chain diacyl phosphatidylcholines that form mixed-interdigitated gel phases: Fourier transform infrared and 2H NMR spectroscopic studies of hydrocarbon chain conformation and orientational order in the liquid-crystalline state, *Biophys. J.*, 1994, **67**, 197–207.
59 M. Bosse, J. Sibold, H. A. Scheidt, L. J. Patalag, K. Kettelhoit, A. Ries, D. B. Werz, C. Steinem and D. Huster, Shiga toxin binding alters lipid packing and the domain structure of Gb3-containing membranes: a solid-state NMR study, *Phys. Chem. Chem. Phys.*, 2019, **21**, 15630–15638.
60 M. F. Brown, Theory of spin-lattice relaxation in lipid bilayers and biological membranes. ^{2}H and ^{14}N quadrupolar relaxation, *J. Chem. Phys.*, 1982, **77**, 1576–1799.
61 G. V. Martinez, E. M. Dykstra, S. Lope-Piedrafita, C. Job and M. F. Brown, NMR elastometry of fluid membranes in the mesoscopic regime, *Phys. Rev. E*, 2002, **66**, 050902.
62 K. Rajamoorthi, H. I. Petrache, T. J. McIntosh and M. F. Brown, Packing and viscoelasticity of polyunsaturated omega-3 and omega-6 lipid bilayers as seen by ^{2}H NMR and X-ray diffraction, *J. Am. Chem. Soc.*, 2005, **127**, 1576–1588.
63 A. Vogel, T. Schröder, C. Lange and D. Huster, Characterization of the myristoyl lipid modification of membrane-bound GCAP-2 by ^{2}H solid-state NMR spectroscopy, *Biochim. Biophys. Acta*, 2007, **1768**, 3171–3181.
64 Y. Elani, S. Purushothaman, P. J. Booth, J. M. Seddon, N. J. Brooks, R. V. Law and O. Ces, Measurements of the effect of membrane asymmetry on the mechanical properties of lipid bilayers, *Chem. Commun.*, 2015, **51**, 6976–6979.
65 A. A. Smith, E. M. Pacull, S. Stecher, P. W. Hildebrand, A. Vogel and D. Huster, Analysis of the dynamics of the human growth hormone secretagogue receptor reveals insights into the energy landscape of the molecule, *Angew. Chem., Int. Ed.*, 2023, **62**, e202302003.